OPEN

Spin excitations of ferronematic order in underdoped cuprate superconductors

G. Seibold[1], C. Di Castro[2], M. Grilli[2] & J. Lorenzana[2]

[1]Institut für Physik, BTU Cottbus-Senftenberg, PBox 101344, 03013 Cottbus, Germany, [2]ISC-CNR, CNISM and Dipartimento di Fisica, Università di Roma ''La Sapienza'', P.le Aldo Moro 5, I-00185 Roma, Italy.

High-temperature superconductors exhibit a characteristic hourglass-shaped spectrum of magnetic fluctuations which most likely contribute to the pairing glue in the cuprates. Recent neutron scattering experiments in strongly underdoped compounds have revealed a significant low energy anisotropy of these fluctuations which we explain by a model in which topological defects of the antiferromagnet clump to producing domain wall segments with ferronematic order. This state does not invoke global charge order but breaks C_4 rotational and inversion symmetry. The incommensurability of the low doping charge-disordered state is in good agreement with experiment and interpolates smoothly with the incommensurability of the stripe phase at higher doping. Within linear spin-wave theory the dynamic structure factor is in very good agreement with inelastic neutron scattering data and can account for the observed energy dependent anisotropy.

There is emerging a coherent picture concerning the structure of spin excitations in strongly underdoped cuprates (for a recent review cf. e.g. Ref. [1]). In both LSCO (with doping less than 5%)[2,3] and YBCO[4–6] materials it is now possible to prepare samples with predominantly one twin domain of the orthorhombic structure which allows to elucidate the symmetry of the magnetic excitations in the CuO_2 planes. Inelastic neutron scattering (INS) experiments[4,7–9] reveal a strongly anisotropic low energy spin response which breaks the four-fold symmetry of a CuO_2 plaquette. The latter is of course also broken due to the orthorhombic distortion, however, for 'conventional' magnetic excitations this would only induce a small redistribution of weight. In cuprates instead, the low energy response is quasi one-dimensional and corresponds to dynamic incommensurate spin modulations which are oriented along the diagonals of a CuO_2 plaquette in LSCO whereas in YBCO the response is oriented along the Cu-O axis. Upon increasing energy these excitations disperse towards the antiferromagnetic wave-vector Q_{AF} which is reached at a characteristic energy E_{cross}. Above E_{cross} the magnetic fluctuations more or less isotropically disperse outwards and approach the antiferromagnetic (AF) spectrum of the undoped compound. On the other hand, a scan in the direction orthogonal to the spin modulation reveals a commensurate response up to E_{cross} whereas for larger energies the excitations start to disperse with almost the same velocity as in the incommensurate modulation direction. Thus the overall magnetic fluctuation spectrum resembles an hourglass parallel to the low energy magnetic spin modulations whereas it is 'Y'-shaped in the orthogonal direction.

Itinerant approaches[10–12] can capture the features of hourglass-shaped excitations, however, it is questionable whether these theories are compatible with the strong energy dependent orientational anisotropies described above. In fact, the consideration of spin excitation anisotropies in detwinned $YBa_2Cu_3O_{6.85}$[13] (i.e. close to optimal doping) already requires an anisotropy of ~3% in the hopping integrals[11] along the two orthorhombic directions. In contrast, close to the metal-insulator transition orthorhombicity alone cannot account for the strong aniso-tropies as also revealed by transport experiments on detwinned samples[14].

The above experimental results are generally well explained by computations of the dynamical structure factor on top of an ordered array of domain walls of the antiferromagnetic order parameter, so-called stripes[15–18]. Not only the hourglass is well described but also general features as, for example, the recovery of C_4 symmetry at high energy[15]. On the other hand a severe problem with this interpretation for strongly underdoped cuprates is the apparent absence of charge order. It has been argued that disorder can 'wash out' the stripe charge correlations and corresponding models of disordered (or fluctuating) stripes have in fact been used in order to describe the magnetic hourglass spectra of cuprates and cobalt oxides[19,20].

Another kind of theories is based on the formation of spin spirals which also break spin rotational invariance similar to stripes, but in the absence of concomitant charge correlations. Early proposals for spirals[21] have been shown to suffer from an intrinsic instability for homogeneous phases manifested by a negative compressibility[22].

On the other hand, holes bound to impurities in the spin glass phase may generate a 'dipolar distortion' in the antiferromagnetic spin background[23] which in turn can stabilize long-range spiral order[24,25]. Such long-range order coexistent with a disordered background is reminiscent of liquid crystal phases[26].

Spin excitations for homogeneous (perfectly ordered) helical magnets have been computed within the tJ-model (see e.g.[27,28]) and analyzed with regard to the magnetic fluctuations in cuprates[29]. However, to the best of our knowledge detailed computations of the dynamical structure factor for spiral ground states on top of a disordered background to compare with experiment have not yet been done.

More recently, we have proposed a state for heavily underdoped cuprates which shares characteristics of both the dipolar and the stripe scenario. Holes added to the antiferromagnet clump in stripe segments ending in fractional vortex-antivortex (VA) pairs[30] resembling disclination pairs in nematics[26]. A single short segment produces a dipolar distortion of the AF background similar to Ref. [23]. Under appropriate conditions a finite density of segments globally breaks C_4 rotational and inversion symmetry and yields spiral long range order, a situation termed ferronematic in Ref. [30]. At large length scales the spin structure coincides with the state proposed in Refs. [24,25], but the microscopic origin of the dipoles, here stemming from the charge segment nematic order, is completely different. In analogy with liquid crystals, at large doping this ferronematic state is expected to transform into a smectic phase thus providing a natural link with the observed stripe state[1] around doping 1/8. In fact, the ferronematic state has the appealing feature that for parameters appropriate for cuprates the resulting magnetic incommensurability coincides with that obtained for static stripes so that a smooth crossover from the former to the latter with doping is feasible.

It has been shown within Gutzwiller variational calculations of Hubbard-type models[30,31] that VA dipoles correspond to stable energy minima for typical cuprate parameters. However, if one is interested only in the spin structure of vortex-antivortex pairs it turns out[30] that the Gutzwiller results can be reproduced within a spin-only (Heisenberg) model supplemented by frustrating interactions in order to stabilize the segments and the induced ferronematic order. Such a model may appear too simplistic to compute dynamical properties. However, our previous experience with ordered stripes[15] shows that it can capture many features of a fully fermionic computation, which in the present case would be restricted to too small sizes to be meaningful.

Thus in order to study excitations on top of the ferronematic ground states our investigations are based on the Heisenberg model

$$H = \sum_{ij} J_{ij} \mathbf{S}_i \mathbf{S}_j \qquad (1)$$

where the spin structure is taken as coplanar and small out-of-plane tilts due to the Dzyaloshinsky-Moriya interaction are neglected. The segments are modeled as a one-dimensional array of N_{va} plaquette centered magnetic vortices with alternating topological charge (cf. Fig. 1a). For a number of N_{seg} segments the total number of holes is given by $N_h = N_{va} N_{seg} v$ where v denotes the 'filling factor' of a segment. Variational Gutzwiller calculations[30] yield $v \approx 0.7$ for diagonal segments.

The following computations are performed for a ratio between next-nearest (J') to nearest (J)-neighbor interaction given by $J'/J = -0.1$. These parameters are fixed in the undoped phase by the condition that the calculated magnon excitations match the measured spin-wave dispersion[32].

Results
We compute the initial spin structure from a linear superposition of randomly positioned vortex-antivortex segments with ferro order as in Ref. [30]
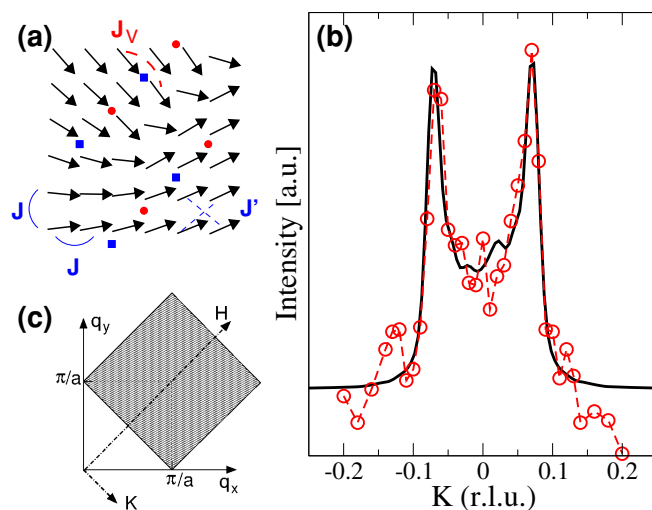
Figure 1 | Static properties of the ferronematic spin structure. (a) Detail of the staggered ferronematic spin arrangement from a 84×84 lattice in the *xy*-plane. Segments are build from plaquette centered vortices (squares) and antivortices (circles) which are stabilized by exchange couplings J_V between diagonally neighbored spins perpendicular to the vortex-antivortex line. Furthermore a nearest-neighbor (J) and next-nearest neighbor (J') coupling is implemented in the model. (b) Fit of the spin structure factor (LSCO) for doping $n_h = 0.05$ and segment length $N_{va} = 4$ perpendicular to the direction of segments. Computations have been done on 84×84 lattices and we average over 10 segment configurations. The experimental resolution (cf. Fig. 4 of Ref. [2]) has been taken into account by convoluting with a gaussian. Data by courtesy of S. Wakimoto. (c) Sketch of the Brillouin zone geometry used in the present paper. The *K*-direction corresponds to the direction of the disordered spiral modulation and the shaded square indicates the momentum range for the intensity plot of Fig. 3.

$$S^x(\mathbf{r}) = S_0 \exp(i\mathbf{Q}\mathbf{r}) \cos \Phi(\mathbf{r})$$
$$S^y(\mathbf{r}) = S_0 \exp(i\mathbf{Q}\mathbf{r}) \sin \Phi(\mathbf{r}) \qquad (2)$$
$$S^z(\mathbf{r}) = 0.$$

Here $\mathbf{Q} = (\pi, \pi)$ is the AF wave-vector and

$$\Phi(\mathbf{r}) = \sum_{n=1}^{N_{seg}} \sum_{i(n)}^{N_{VA}} (-1)^{i(n)} \arctan\left(\frac{x - x_{i(n)} - 0.5}{y - y_{i(n)} - 0.5}\right) \qquad (3)$$

is the angular spin distortion due to the N_{seg} segments. In Eq. (3) the sum over $i(n)$ is due to sites belonging to segment n and $(-1)^{i(n)} = 1(-1)$ corresponds to a plaquette centered magnetic (anti)vortex. Then the classical energy of Eq. (1) is minimized where the VA structure is stabilized by an additional coupling J_V between diagonally neighbored spins across the segments (cf. Fig. 1a). A fit of the VA structure to the result of a Gutzwiller variational computation yields $J_V/J = 8$ (cf. Methods section). In order to account for fluctuations beyond the variational result we take a smaller value $J_V/J = 1.5$ which induces the same winding number for the ferronematic spiral as for $J_V/J = 8$ (cf. supplementary information) and reproduces the low doping magnetic incommensurability of LSCO. Thus this parameter is fixed at the static level and there are no free parameters in the following dynamical computations.

For doping of $n_h = 0.05$ Fig. 1b demonstrates that this approach can reproduce the static spin structure factor of LSCO measured with elastic neutron scattering. Note that the present fit with plaquette centered vortices yields shorter segments with $N_{va} = 4$ as compared to our previous investigations[30] with site-centered vortex-antivortex pairs.
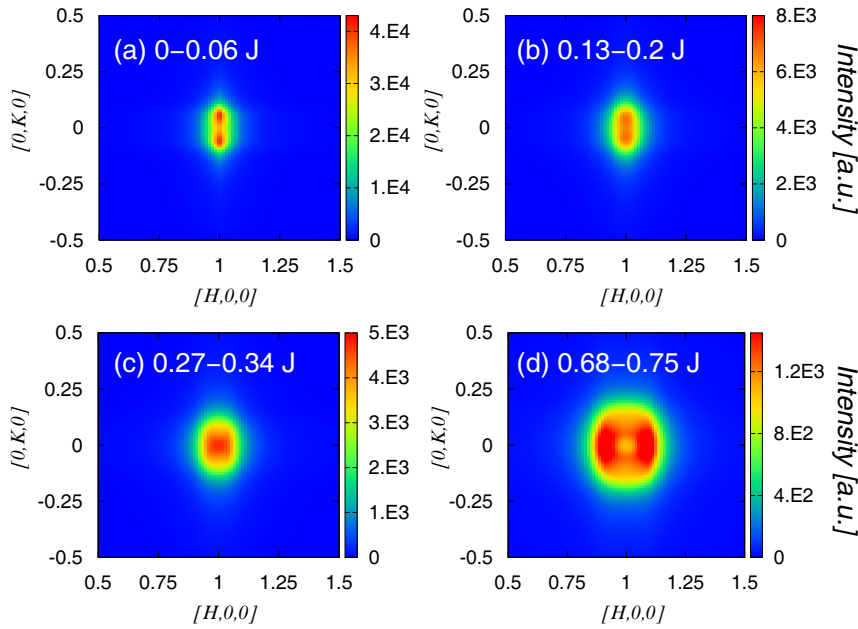
Figure 2 | Neutron scattering intensity for the ferronematic at doping $n_h = 0.05$. The magnetic neutron-scattering cross section has been integrated over energy ranges (a) 0–0.06 J, (b) 0.13–0.2 J, (c) 0.27–0.34 J, (d) 0.68–0.75 J. The momentum range corresponds to the shaded area indicated in Fig. 1c. The value of the perpendicular momentum q_z has been calculated from energy-momentum conservation for an incident neutron beam energy with $E_i = 0.3$ J (panels a,b) and $E_i = 0.8$ J (panels c,d). Average over 6 configurations.

In order to compute excitations on top of the ferronematic ground state we rotate the spin quantization axis to the direction of the local mean-field magnetization and apply linear spin-wave theory as described in Methods.

It is then straightforward to obtain the spin susceptibilities $\chi_{ij}^{\alpha\beta}(\omega) = \left\langle \left\langle S_i^\alpha; S_j^\beta \right\rangle \right\rangle$ from the equations of motion and to compute the Fourier transformed

$$\chi_{\mathbf{q}}^{\alpha\beta}(\omega) = \frac{1}{N} \sum_{ij} e^{i\mathbf{q}\cdot(\mathbf{R}_i - \mathbf{R}_j)} \left\langle \chi_{ij}^{\alpha\beta}(\omega) \right\rangle_{config.}. \quad (4)$$

In practice we evaluate $\chi_{\mathbf{q}}^{\alpha\beta}(\omega)$ for a randomly generated configuration of segments and then take the average over typically 10–20 configurations as indicated by $\langle \ldots \rangle_{config.}$.

The spins of the ferronematic state can fluctuate both in- and out-of the CuO_2 plane. Both types of excitations contribute to the magnetic neutron-scattering cross section measured by INS which is proportional to

$$\frac{d^2\sigma}{d\Omega dE} \sim \sum_{\alpha\beta} \frac{1}{q^2} \left(q^2 \delta_{\alpha\beta} - q_\alpha q_\beta\right) Im\chi^{\alpha\beta}(\mathbf{q}, \omega) \equiv S_{\mathbf{q}}(\omega). \quad (5)$$

Here $\chi^{\alpha\beta}(\mathbf{q}, \omega)$ only depends on the in-plane components of $\mathbf{q}$ while the perpendicular component q_z enters the cross section only through the prefactors inside the sum. In the extreme case that the q_z is much larger than the in-plane components (i.e. for the case that the neutron beam is almost perpendicular to the CuO_2 plane and high energies) the response is dominated by the in-plane response $\chi_{\mathbf{q}}^{\parallel}(\omega)$[33]. In practice, q_z depends on energy and one always has a contribution from perpendicular, in-plane and off-diagonal susceptibilities which we have all included. In our computations we assumed an incoming neutron energy E_i and a scattering geometry as in typical neutron scattering experiments (i.e. q_x and q_y in the first Brillouin zone).

Fig. 2 shows momentum cuts of the neutron scattering intensity within different energy ranges which have been obtained from the same ferronematic configurations for which the static response in Fig. 1b has been evaluated. Momentum cuts along the H- and

K-direction for the same energies are reported in Fig. 3. At low energies (panel (a) in Figs. 2, 3) the response is dominated by two incommensurate peaks along the orthorhombic K-direction due to the spiral modulation perpendicular to the segments and coinciding in momentum space with the static peaks in Fig. 1b. The period of the modulation is obtained as $\lambda = 2\pi/|q_K| = 14a_{ortho}$ corresponding to an incommensurability of $\varepsilon^{ortho} = 1/14 = 0.07143$. Note that for diagonal stripes with v holes per site the incommensurability would be given by $\varepsilon^{ortho} = n_h/v$ thus yielding the same value for $n_h = 0.05$ and $v = 0.7$.

Upon increasing energy the reponse first keeps the elongated shape along the K-direction (panel b) but becomes more isotropic at higher energies (panel c). From the momentum cuts in Fig. 3 the
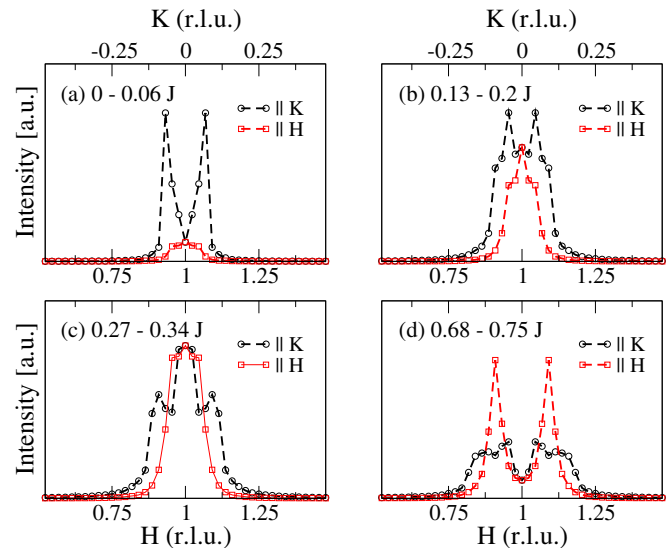
Figure 3 | Momentum cuts parallel (H-direction, red squares) and perpendicular to the segments (K-direction, black circles) for the intensity distributions shown in Fig. 2.

3
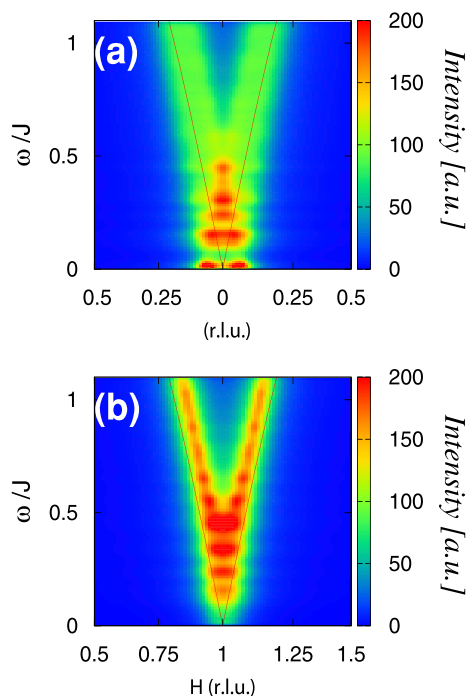
Figure 4 | Intensity plot of the cross section $\omega S_q(\omega)$ [Eq. (5)] for a momentum cut perpendicular (panel a) and parallel (panel b) to the segments. The value of the perpendicular momentum q_z has been calculated from energy-momentum conservation for an incident neutron beam energy with $E_i = J$. The solid lines report the magnon dispersion of the undoped antiferromagnet. Average over 6 configurations.

dispersion of excitations along the K-direction toward the antiferromagnetic wave-vector can be clearly deduced. Panels b,c of Fig. 3 also reveal a small shoulder in the momentum structure along K which is due to an outwards dispersing branch. Similar to the case of stripes[16] and enhanced by disorder the corresponding intensity is strongly reduced with respect to the inwards dispersing excitations.

At still higher energies the magnetic scattering intensity acquires a quasi two-dimensional ring-shaped structure (Fig. 2, panel d). The overall features of the intensity distribution are rather similar to data from INS experiments on LSCO (cf. Fig. 1 in Ref. [9]), however, our calculations reveal an anisotropic intensity distribution with variable weight ratio between the H- and K-directions at different energy ranges. (cf. panel (c) of Fig. 3). This feature resembles an analogous rotation of weight observed in the magnetic scattering from static stripes in $La_{1.875}Ba_{0.125}CuO_4$[34], whereas the data from strongly underdoped LSCO seem to indicate a more isotropic distribution of weight. We should remark that for the case of stripes we observe that a computation in a spin only model (as here) yields a more anisotropic response than a more accurate computation in a fermion model[15]. Thus we attribute this small difference in anisotropy to the simplicity of the model. Unfortunately a fermion model could not be used due to the large size required to take into account disorder with high momentum resolution.

The magnetic dispersions along K and H directions can be deduced from Fig. 4 which shows the corresponding cuts of the magnetic structure factor Eq. (5) weighted by energy. Panel (a) of Fig. 4 clearly reveals the basic features of the hourglass spectrum although the resolution is limited due to the large periodicity of the ferronematic spiral as compared to the size of the lattice which can be dealt with. The large intensity feature corresponds to the inwards dispersing magnetic excitations which merge at Q_{AF} and subsequently disperse outwards again with reduced intensity. At high energies the magnetic fluctuations approach the magnon dispersion
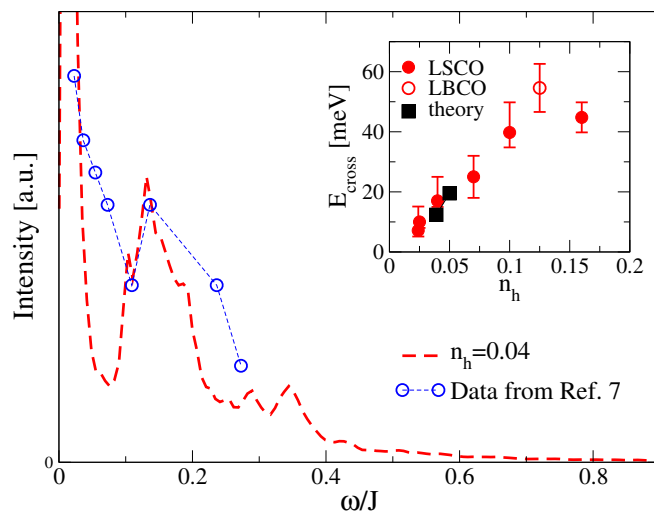

Figure 5 | Energy dependence of the magnetic cross section $S_{q=Q_{AF}}(\omega)$ (cf. Eq. (5)) at the antiferromagnetic wave-vector. The main panel reports $S_{q=Q_{AF}}(\omega)$ for doping $x = 0.04$ (dashed) together with experimental data extracted from Fig. 1 of Ref. [7]. Inset: Comparison of the crossing energy with experimental data for LSCO (solid circles) and LBCO (open circle) from Ref. [8]. For the conversion into energy units we use $J = 112$ meV[32] and a frequency independent renormalization factor $Z_c = 1.18$[35].

of the undoped antiferromagnet which is indicated by the solid line in Fig. 4. The Y-shaped structure of the spin excitations in the parallel direction to the segments is reported in panel (b) of Fig. 4. Here the low energy magnetic excitations are confined to Q_{AF} but also start to follow those of the undoped AF above the crossing energy E_{cross}.

The location of E_{cross} is difficult to determine from Fig. 4 due to the limited resolution. Instead we deduce this scale from the energy dependence of the magnetic structure factor for the antiferromagnetic wave vector Q_{AF} which is shown in Fig. 5 for doping $x = 0.04$. Since the ferronematic spin spiral is strongly disordered the static structure factor also displays small but finite weight at Q_{AF}. This induces a 'quasi-elastic' peak at $\omega \to 0$ in the frequency dependent magnetic cross section, $S_{q=Q_{AF}}(\omega)$ in addition to the higher energy feature at $E_{cross} \approx 0.14$ J. We can convert the 'J-scale' into energy units by taking $J = 112$ meV[32] and a frequency independent renormalization factor $Z_c = 1.18$[35] which yields good agreement with the magnon dispersion of the undoped AF. Based on this conversion we also show in Fig. 5 experimental $S_{q=Q_{AF}}(\omega)$ data for $La_{1.96}Sr_{0.04}CuO_4$ which we have extracted from Fig. 1 of Ref. [7]. Interestingly also these data support an increase of $S_{q=Q_{AF}}(\omega)$ for $\omega \to 0$ in agreement with the persistence of AF domains in an otherwise incommensurate ordered spin system. Finally, the inset to Fig. 5 reports E_{cross} for $x = 0.04$ and $x = 0.05$ which fits rather well into the experimentally determined[8] evolution of E_{cross} with doping. In contrast, stripe calculations in the strongly underdoped regime usually significantly overestimate E_{cross}[17] although this may also be cured by disorder[19].

Discussion

We have shown that the spectrum of spin excitations computed on top of a ferronematic ground state is in qualitative and quantitative agreement with inelastic neutron scattering experiments on cuprate superconductors in the spin glass phase. Since the ferronematic also can be thought of arising from melted stripes our theory provides an explanation for the continuous evolution of the hourglass-shaped magnetic excitations from low to optimal doping. It should be mentioned that preliminary Monte-Carlo simulations also seem to
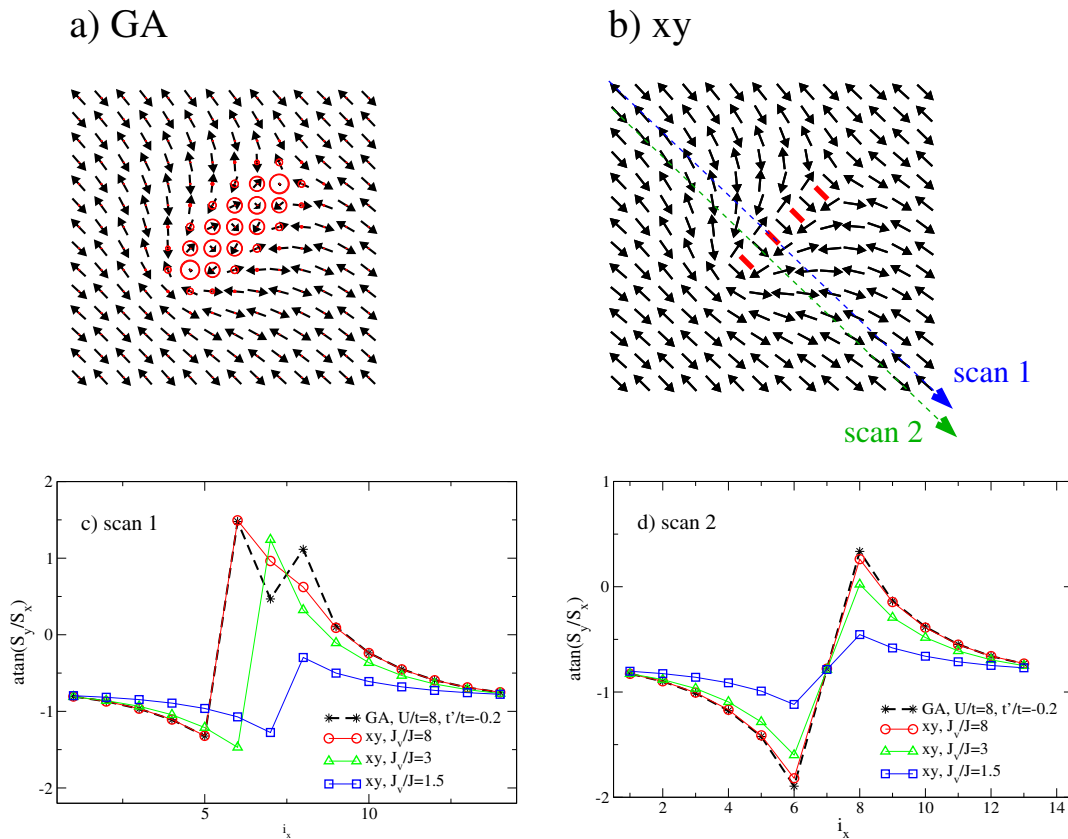
Figure 6 | Comparison of spin textures obtained from the Hubbard model within the GA (a) and the Heisenberg model (b) The GA solution shown in panel (a) has been obtained for 4 holes in a 14 × 14 system. Parameters: $U/t = 8$, $t'/t = -0.2$. The spin structure of panel (b) results from the minimization of the Heisenberg model. Here the 4 diagonal exchange couplings which are indicated by bars are set to $J_v/J = 8$ and all other nearest-neighbor couplings are $J'/J = -0.1$. Panels (c), (d) compare the angular rotation of the spins ($= atan(S_y/S_x)$) along the scans indicated in panel (b).

support smectic charge correlations which are stabilized by long-range Coulomb interactions. While such correlations between disordered stripes can also induce an incommensurate magnetic response[19], the magnetic fluctuations of the ferronematic spiral are due to the disordered magnetic background which is induced by the vortex and antivortex dipoles of the charge segments.

Experimentally, the ferronematic state is supported by the observation of a low temperature ferroelectric phase in the spin glass phase of cuprates[36]. In fact, the ferronematic state breaks inversion symmetry so that on general grounds[37] a ferroelectric distortion becomes possible e.g. via the inverse Dzyaloshinskii-Moriya mechanism[38]. The 'smoking gun' experiment would then be to test whether the onset temperature of incommensurate spin fluctuations coincides with that of the ferroelectric as predicted by our model.

Methods

Parameters for the effective Heisenberg model. In order to estimate the effective coupling J_v across the plaquette centered magnetic vortices and antivortices (cf. Fig. 1) we perform a variational calculation based on the single-band Hubbard model

$$H = \sum_{ij,\sigma} t_{ij} c_{i,\sigma}^\dagger c_{j,\sigma} + U \sum_i n_{i,\uparrow} n_{i,\downarrow} \qquad (6)$$

including nearest-neighbor (t) and next-nearest neighbor (t') hopping. Ground state properties are obtained from the Gutzwiller variational wave-function $\langle \Psi_G| = \hat{P}_G |\Phi_0\rangle$ where $\hat{P}_G = \Pi_i \left[1 - (1 - g_i) n_{i,\uparrow} n_{i,\downarrow} \right]$ partially projects out doubly occupied sites from the Slater determinant $|\Phi_0\rangle$. We evaluate $E_G(\{g_i\}) = \langle \Psi_G|H|\Psi_G\rangle/\langle \Psi_G|\Psi_G\rangle$ in the limit of infinite dimensions[39] corresponding to the so-called Gutzwiller approximation (GA) and minimize with respect to the variational parameters g_i. We set $U/t = 8$ and $t'/t = -0.2$ which within a time-dependent extension of the GA reproduces the spin-excitations of undoped LSCO[15,16].

Panel (a) of Fig. 6 reports the spin/charge texture obtained in this way for 4 holes (192 particles) on a 14 × 14 lattice with periodic boundary conditions. Hole charges

(indicated by circles) are arranged in 2 × 2 plaquettes aligned along the diagonal direction. The center of the plaquettes alternately contains a magnetic vortex and antivortex, respectively, inducing a phase change of the AF order across the segment. This feature can be modeled within the Heisenberg model by diagonal couplings J_v indicated by solid bars in panel (b) of Fig. 6. Panels (c,d) compare the angular spin twist $\sim atan(S_y/S_x)$ between GA computation and minimization of the Heisenberg model energy along the two scans indicated in panel (b). We find that for $J_v/J = 8$ there is excellent agreement of the spin far field (which is determined by the dipole strength of the segment) between both approaches. On the other hand, one may argue that the variational GA overestimates the localization of hole charges and that including corrections beyond the GA would lead to actually smaller values of J_v/J. The phase change across the segment is then reduced for smaller J_v/J as can be seen from panels (c,d). However, as long as $J_v/J \gtrsim 1.5$ we find that the static and dynamic spin structure factor only weakly depends on J_v/J as demonstrated in the supplementary material where we show results for the GA fitted value $J_v/J = 8$. In the 'Results' section instead we have taken a smaller value $J_v/J = 1.5$ in order to include fluctuations beyond the GA variational approach.

Evaluation of spin excitations. Spin excitations on top of the ferronematic ground state are obtained by applying a rotation to the spins

$$S_i^x = \tilde{S}_i^x \cos(\Theta_i) + \tilde{S}_i^y \sin(\Theta_i) \qquad (7)$$

$$S_i^y = \tilde{S}_i^y \cos(\Theta_i) + \tilde{S}_i^x \sin(\Theta_i) \qquad (8)$$

$$S_i^z = \tilde{S}_i^z \qquad (9)$$

so that the spin quantization axis points in the direction of the local mean-field magnetization[40].

For this effective ferromagnetic state one can apply the Holstein-Primakoff transformation:

$$\tilde{S}_i^x = \frac{1}{2} \left(a_i^\dagger + a_i \right)$$

$$\tilde{S}_i^y = -\frac{1}{2} + a_i^\dagger a_i$$

$$\tilde{S}_i^z = \frac{1}{2i}\left(a_i^\dagger - a_i\right).$$

The linear-spin wave theory Hamiltonian reads,

$$H = \sum_{ij} A_{ij} a_i^\dagger a_j + \frac{1}{2}\sum_{ij} B_{ij}\left[a_i^\dagger a_j^\dagger + a_j a_i\right] \quad (10)$$

with

$$A_{ii} = -\sum_j J_{ij}\cos(\Theta_i - \Theta_j) \quad (11)$$

$$A_{i\neq j} = \frac{1}{2}J_{ij}\left[\cos(\Theta_i - \Theta_j) + 1\right] \quad (12)$$

$$B_{ij} = \frac{1}{2}J_{ij}\left[\cos(\Theta_i - \Theta_j) - 1\right] \quad (13)$$

where Θ_i is the angle the spin i forms with the x-axis. Here we used the fact that the configurations are coplanar. The absence of unstable spin-wave modes in our analysis supports this assumption.

1. Fujita, M. *et al.* Progress in Neutron Scattering Studies of Spin Excitations in High-Tc Cuprates. *J. Phys. Soc. Jpn.* **81**, 011007 (2012).
2. Wakimoto, S. *et al.* Direct observation of a one-dimensional static spin modulation in insulating $La_{1.95}Sr_{0.05}CuO_4$. *Phys. Rev. B* **61**, 3699 (2000).
3. Matsuda, M. *et al.* Static and dynamic spin correlations in the spin-glass phase of slightly doped $La_{2-x}Sr_xCuO_4$. *Phys. Rev. B* **62**, 9148 (2000).
4. Hinkov, V. *et al.* Electronic Liquid Crystal State in the High-Temperature Superconductor $YBa_2Cu_3O_{6.45}$. *Science* **319**, 597 (2008).
5. Haug, D. *et al.* Neutron scattering study of the magnetic phase diagram of underdoped $YBa_2Cu_3O_{6+x}$. *New J. Phys.*, **12**, 105006 (2010).
6. Daou, R. *et al.* Broken rotational symmetry in the pseudogap phase of a high-Tc superconductor. *Nature* **463**, 519 (2010).
7. Matsuda, M. *et al.* Magnetic Dispersion of the Diagonal Incommensurate Phase in Lightly Doped $La_{2x}Sr_xCuO_4$. *Phys. Rev. Lett.* **101**, 197001 (2008).
8. Matsuda, M., Fernandez-Baca, J. A., Fujita, M., Yamada, K. & Tranquada, J. M. Detailed structure of the low-energy magnetic dispersion of the diagonal incommensurate phase in $La_{1.975}Sr_{0.025}CuO_4$. *Phys. Rev. B* **84**, 104524 (2011).
9. Matsuda, M., Granroth, G. E., Fujita, M., Yamada, K. & Tranquada, J. M. Energy-dependent crossover from anisotropic to isotropic magnetic dispersion in lightly doped $La_{1.96}Sr_{0.04}CuO_4$. *Phys. Rev. B* **87**, 054508 (2013).
10. Norman, M. R. Relation of neutron incommensurability to electronic structure in high-temperature superconductors. *Phys. Rev. B* **61**, 14751 (2000).
11. Eremin, I. & Manske, D. Fermi-Liquid-Based Theory for the In-Plane Magnetic Anisotropy in Untwinned High-Tc Superconductors. *Phys. Rev. Lett.* **94**, 067006 (2005).
12. Sherman, A. & Schreiber, M. Low-frequency incommensurate magnetic response in strongly correlated systems. *Phys. Rev. B* **69**, 100505 (2004).
13. Hinkov, V. *et al.* Two-dimensional geometry of spin excitations in the high-transition-temperature superconductor $YBa_2Cu_3O_{6+x}$. *Nature* **430**, 650 (2004).
14. Ando, Y., Segawa, K., Komiya, S. & Lavrov, A. N. Electrical Resistivity Anisotropy from Self-Organized One Dimensionality in High-Temperature Superconductors. *Phys. Rev. Lett.* **88**, 137005 (2002).
15. Seibold, G. & Lorenzana, J. Doping dependence of spin excitations in the stripe phase of high-Tc superconductors. *Phys. Rev. B* **73**, 144515 (2006).
16. Seibold, G. & Lorenzana, J. Magnetic Fluctuations of Stripes in the High Temperature Cuprate Superconductors. *Phys. Rev. Lett.* **94**, 107006 (2005).
17. Seibold, G. & Lorenzana, J. Calculation of incommensurability and spin excitations of diagonal stripes in underdoped lanthanum cuprates. *Phys. Rev. B* **80**, 012509 (2009).
18. Seibold, G., Markiewicz, R. S. & Lorenzana, J. Spin canting as a result of the competition between stripes and spirals in cuprates. *Phys. Rev. B* **83**, 205108 (2011).
19. Vojta, M., Vojta, T. & Kaul, R. K. Spin Excitations in Fluctuating Stripe Phases of Doped Cuprate Superconductors. *Phys. Rev. Lett.* **97**, 097001 (2006).
20. Andrade, E. C. & Vojta, M. Disorder, Cluster Spin Glass, and Hourglass Spectra in Striped Magnetic Insulators. *Phys. Rev. Lett.* **109**, 147201 (2012).
21. Shraiman, B. I. & Siggia, E. D. Spiral phase of a doped quantum antiferromagnet. *Phys. Rev. Lett.* **62**, 1564 (1989).
22. Auerbach, A. & Larson, B. E. Doped antiferromagnet: The instability of homogeneous magnetic phases. *Phys. Rev. B* **43**, 7800 (1991).
23. Aharony, A., Birgeneau, R. J., Coniglio, A., Kastner, M. A. & Stanley, H. E. Magnetic phase diagram and magnetic pairing in doped La_2CuO_4. *Phys. Rev. Lett.* **60**, 1330 (1988).
24. Hasselmann, N., Castro Neto, A. H. & Morais Smith, C. Topological defects and the spin glass phase of cuprates. *Europhys. Lett.* **56**, 870 (2001).
25. Sushkov, O. P. & Kotov, V. N. Theory of Incommensurate Magnetic Correlations Across the Insulator-Superconductor Transition of Underdoped $La_{2x}Sr_xCuO_4$. *Phys. Rev. Lett.* **94**, 097005 (2005).
26. Chaikin, P. M. & Lubensky, T. C. *Principles of Condensed Matter Physics.* Cambridge University Press, Cambridge, 1995.
27. Gan, J., Andrei, N. & Coleman, P. Spin waves in a doped antiferromagnet. *J. Phys.: Condens. Matter* **3**, 3537 (1991).
28. Shraiman, B. I. & Siggia, E. D. Excitation spectrum of the spiral state of a doped antiferromagnet. *Phys. Rev. B* **46**, 8305 (1992).
29. Milstein, A. I. & Sushkov, O. P. Effective field theories and spin-wave excitations in helical magnets. *Phys. Rev. B* **84**, 195138 (2011).
30. Seibold, G., Capati, M., Di Castro, C., Grilli, M. & Lorenzana, J. Hidden ferronematic order in underdoped cuprates. *Phys. Rev. B* **87**, 035138 (2013).
31. Seibold, G. Vortex, Skyrmion, and elliptical domain-wall textures in the two-dimensional Hubbard model. *Phys. Rev. B* **58**, 15520 (1998).
32. Coldea, R. *et al.* Spin Waves and Electronic Interactions in La_2CuO_4. *Phys. Rev. Lett.* **86**, 5377 (2001).
33. Lorenzana, J., Seibold, G. & Coldea, R. Sum rules and missing spectral weight in magnetic neutron scattering in the cuprates. *Phys. Rev. B* **72**, 224511 (2005).
34. Tranquada, J. M. *et al.* Quantum magnetic excitations from stripes in copper oxide superconductors. *Nature* **429**, 534 (2004).
35. Singh, R. R. P. Thermodynamic parameters of the $T = 0$, spin-1/2 square-lattice Heisenberg antiferromagnet. *Phys. Rev. B* **39**, 9760 (1989).
36. Viskadourakis, Z. *et al.* Low-temperature ferroelectric phase and magnetoelectric coupling in underdoped La_2CuO_{4+x}. *Phys. Rev. B* **85**, 214502 (2012).
37. Mostovoy, M. Ferroelectricity in Spiral Magnets. *Phys. Rev. Lett.* **96**, 067601 (2006).
38. Sergienko, I. A. & Dagotto, E. Role of the Dzyaloshinskii-Moriya interaction in multiferroic perovskites. *Phys. Rev. B* **73**, 094434 (2006).
39. Gebhard, F. Gutzwiller correlated wave functions in finite dimensions d: A systematic expansion in 1/d. *Phys. Rev. B* **41**, 9452 (1990).
40. Merino, J., McKenzie, Ross, H., Marston, J. B. & Chung, C. H. The Heisenberg antiferromagnet on an anisotropic triangular lattice: linear spin-wave theory. *J. Phys.: Condens. Matter* **11**, 2965 (1999).

Acknowledgments

Author contributions

G.S. developed the numerical code and wrote the manuscript; G.S., C.D.C., M.G. and J.L. contributed to analyze the results and write the manuscript.

Additional information